ICARUS **124,** 586–597 (1996)
ARTICLE NO. 0232

Retrieval of Atmospheric Temperatures in the Martian Planetary Boundary Layer Using Upward-Looking Infrared Spectra

MICHAEL D. SMITH

NRC, NASA/Goddard Space Flight Center, Code 693, Greenbelt, Maryland 20771
E-mail: michael@chryse.gsfc.nasa.gov

BARNEY J. CONRATH AND JOHN C. PEARL

NASA/Goddard Space Flight Center, Code 693, Greenbelt, Maryland 20771

AND

EUGENE A. USTINOV

Department of Astronomy, Cornell University, Ithaca, New York 14853

Received February 9, 1996; revised June 27, 1996

We present an algorithm for the retrieval of temperature in the planetary boundary layer (lowest few kilometers) of the martian atmosphere using upward-looking infrared spectra from a Mars lander. Temperature profiles retrieved from an orbiting or passing spacecraft do not have adequate vertical resolution to provide significant information within the planetary boundary layer. By using spectra taken from a surface lander looking upward toward zenith, and by transforming to a vertical coordinate that "stretches out" the atmosphere just above the surface where the contribution to the observed radiation peaks, we find that an efficient algorithm can be formulated with adequate vertical resolution to successfully retrieve temperature profiles that exhibit the major features of the diurnal cycle of planetary boundary layer temperatures. We expect that this technique can be extended to simultaneously retrieve the opacity, and possibly the scattering properties, of atmospheric aerosols as well. Although no upward-looking martian infrared spectra yet exist, demonstration of the abilities of a lander-based infrared spectrometer is important for the planning of future missions to Mars.

1. INTRODUCTION

The practice of retrieving planetary atmospheric temperature profiles from thermal infrared spectra taken by a passing or orbiting spacecraft has been well established. If the atmospheric opacity source shows frequency dependent absorption, such as a molecular absorption line, then different levels of the atmosphere may be sampled by recording the radiance at several different frequencies. If the vertical variation of temperature and opacity is not too great, then the observed radiance will be characteristic of the temperature in a layer centered near the level where the absorber optical depth as measured along the line of sight from the observer (spacecraft) reaches unity. When opacity varies with frequency, the height in the atmosphere at which unit optical depth is reached is different for different frequencies. By using this fact, a temperature profile can be retrieved if the vertical distribution of the opacity source is known.

In the case of the martian atmosphere, thermal infrared spectra were obtained by the orbiting Mariner 9 Infrared Interferometer Spectrometer (IRIS) instrument during 1971 and 1972. A description of the Mariner 9 IRIS instrument is given by Hanel *et al.* (1972a). In the IRIS spectra, there is a strong CO_2 absorption centered at 667 cm^{-1} (15 μm) that is suitable for temperature retrieval, and a broad, weaker silicate absorption centered at about 1050 cm^{-1} (9–10 μm) caused primarily by dust suspended in the atmosphere. Using the CO_2 absorption band, the Mariner 9 IRIS data set has been used to retrieve atmospheric temperature profiles (for example, Hanel *et al.* 1972b; Conrath *et al.* 1973; and Conrath 1975; 1981). The broad silicate absorption has been used to retrieve dust properties from Mariner 9 IRIS data set (for example, Toon *et al.* 1977; Santee and Crisp 1993).

The process of retrieving temperature profiles from infrared spectra taken from an orbiting or passing spacecraft is powerful, but the vertical resolution of the retrieved profiles is limited by the width of the region from which

0019-1035/96 $18.00

radiation at a given frequency originates. For the 667-cm^{-1} CO_2 band, Conrath (1972) finds that this ranges from about half of a scale height near the surface to two scale heights at the highest retrieved levels. This vertical resolution still provides very useful information for many investigations, but it is not high enough for studies involving the martian planetary boundary layer. The limiting vertical resolution can be improved slightly by better signal-to-noise (Conrath 1972), but there is still a fundamental limit to the highest vertical resolution obtainable, even with noise-free data, which results from the ill-posed nature of the inverse radiative transfer problem. However, if instead of taking spectra from a spacecraft above the atmosphere looking downward, we take spectra from a lander on the planet surface looking upward to the sky, then much higher vertical resolution can be obtained in the lowest few kilometers of the atmosphere.

In this paper, we present a new algorithm for the retrieval of temperature profiles in the lowest few kilometers of the atmosphere with high vertical resolution, using thermal infrared spectra taken by an upward-looking, lander-based spectrometer on the surface of Mars. There was no instrument on the Viking lander spacecraft capable of such an observation, so no upward-looking spectra now exist. However, an upward-looking spectrometer could be placed on a future Mars lander, and here we demonstrate the important capabilities of such an instrument. In the next section we give some background material on the martian planetary boundary layer, and on the infrared spectra and weighting functions expected to be observed from a lander on the surface. In Section 3 we describe the algorithm that we use to retrieve temperatures, and in Section 4 we present the results of retrievals from synthetic data. Finally, in Section 5 we discuss some problems and issues related to the algorithm, and in Section 6 we summarize our findings.

2. BACKGROUND

a. The Martian Planetary Boundary Layer and Its Diurnal Variation

On Mars, the planetary boundary layer (PBL) occupies the lowest few kilometers of the atmosphere. The PBL is characterized by a large change in temperatures from day to night, with convective mixing during the day, and a stable inversion layer with a very large temperature gradient at night. Although a significant fraction of the mass of the atmosphere lies within the PBL, there are very few direct measurements of meteorological parameters in this region. The two Viking Landers directly measured temperature between 3.5 and 1.5 km during their descent (Seiff and Kirk 1977), and after landing measured temperature, pressure, and wind velocity, but only at one height (1.6 m) above the surface (Hess *et al.* 1977, Sutton *et al.* 1978). Radio occultation experiments by Mariner 9 (Kliore *et al.* 1973) and the Viking Orbiters (Lindal *et al.* 1979) provide temperature profiles at scattered locations and times within the PBL. In addition, observations of clouds in Viking images allow indirect inferences to be made about some PBL properties in a few instances (Kahn 1984).

Atmospheric temperature profiles, the abundance of dust and water ice aerosols, and wind velocity are the key quantities necessary for dynamical modeling of the PBL. Current numerical models of the PBL (for example, Haberle *et al.* 1993; Savijärvi 1995) are limited by the lack of observations against which to compare. The fluxes of heat, mass, and momentum in the PBL are important drivers for the rest of the atmosphere, and the determination of these fluxes is one of the chief goals of PBL modeling. PBL modeling can also shed light on the processes that exchange volatiles, such as CO_2 and H_2O, across the surface-atmosphere interface. The conditions under which dust can be raised from the surface and then transported is another important area of research that requires detailed knowledge of PBL processes. Clearly, temperature profiles of the lower atmosphere with high vertical resolution would be a very valuable addition to the current set of PBL data, and would provide a set of ''ground-truth'' observations against which models could be tested.

To demonstrate our retrieval algorithm we require a set of ''typical'' temperature profiles through the martian PBL that captures the main expected vertical and diurnal variations. Radiative-convective modeling by Gierasch and Goody (1967, 1968) and by Pollack *et al.* (1979) gives typical temperature profiles for various different times during the martian day. More recently, detailed models of the PBL including surface-atmosphere interactions have been attempted (for example, Haberle *et al.* 1993; Savijärvi 1991, 1995). Guided by the profiles from these models, from the post-Viking standard martian atmosphere of Seiff (1982), and by the observations described earlier, we adopt the set of temperature profiles displayed in Fig. 1 as our nominal PBL temperature profiles.

The temperature profiles displayed in Fig. 1 show the main vertical and diurnal variations of PBL temperatures predicted by modeling. For convenience, we describe local solar time by arbitrarily dividing the martian day (or ''sol'') into 24 martian hours. From late morning until sunset (1100–1800 hours) the convective portion of the atmosphere extends upward from the surface for several kilometers. The temperature profile is taken to be nearly an adiabat but slightly stable based on descent probe measurements (Seiff and Kirk 1977). After the sun sets, a strong inversion layer quickly forms near the surface and grows to a depth of about 1 km by dawn (0600 hours). During the morning hours (0800–1100), the convective region once again builds upward from the surface, briefly forming a small local minimum in the temperature profile below 1

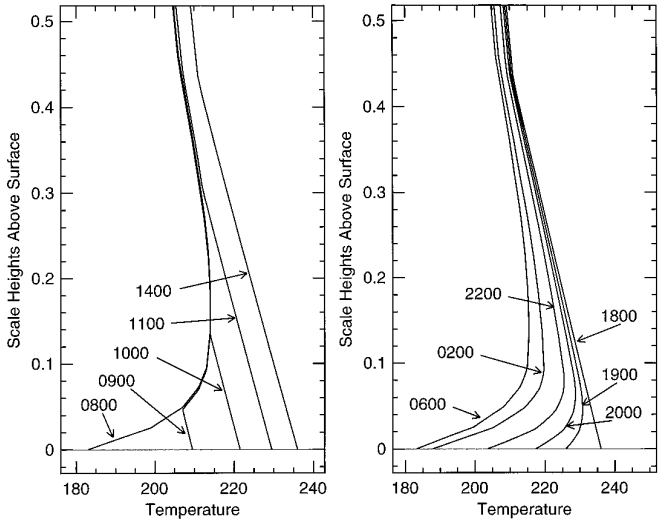

FIG. 1. Nominal model temperature profiles for various times throughout the martian day. Daytime temperature profiles are shown in the left panel, nighttime temperature profiles are shown in the right panel. A scale height at these temperatures on Mars is approximately 11 km.

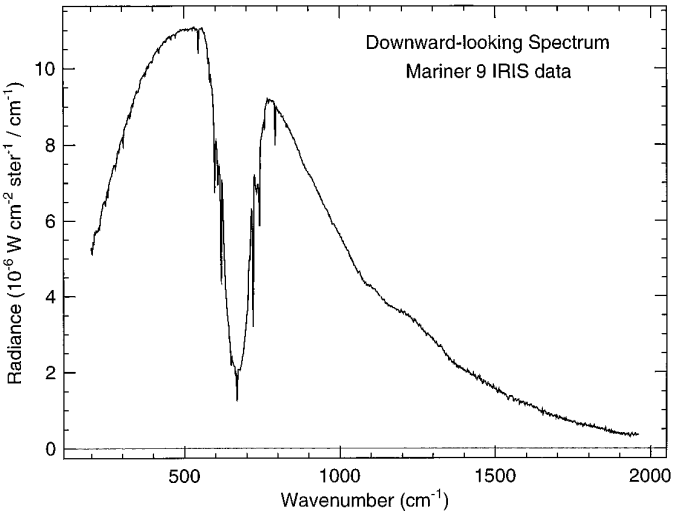

FIG. 2. A typical downward-looking Mars infrared spectrum taken by the Mariner 9 IRIS instrument. This is the average of six spectra taken on revolution 174 (L_s = 336°) with similar location (−23° latitude, 29° longitude), emission angle (13°), and time of day (1400 hours). The effective spectral resolution of Mariner 9 IRIS spectra is 2.8 cm^{-1}. By this time the large dust storm that enshrouded the planet on the arrival of Mariner 9 had subsided.

km above the surface. The large diurnal variation of temperature is confined to the lowest half scale height of the atmosphere. From Fig. 1 it is apparent that to characterize even the major features of the diurnal variation in the PBL it is necessary to resolve features as small as a few hundred meters (a few hundredths of a scale height), which is a vertical scale far smaller than can be retrieved from spectra taken from an orbiting or passing spacecraft.

b. Upward-Looking and Downward-Looking Infrared Spectra of Mars

We will refer to a spectrum as observed from above the atmosphere looking downward at the planet surface as a "downward-looking" spectrum, and to a spectrum as observed from the surface looking upward toward the sky as an "upward-looking" spectrum. Figure 2 shows a typical downward-looking infrared spectrum of Mars. Except for the strong CO_2 absorption feature centered at 667 cm^{-1}, and a broad, relatively weak silicate absorption centered at about 1050 cm^{-1}, the spectrum is well characterized by the shape of a Planck function at the surface temperature of 275 K.

Figure 3 shows synthetic upward-looking spectra of Mars using temperature profiles typical of various times during the martian day (see Fig. 1). To obtain these spectra we assume a dust-free non-scattering atmosphere in local thermodynamic equilibrium. In Fig. 3, radiation coming from CO_2 absorption and re-emission is seen. In the optically thick portions of the spectrum (~640–700 cm^{-1}) the radiance has a brightness temperature characteristic of the lowest few hundred meters of the atmosphere. The center of the CO_2 band at 667 cm^{-1} is seen in absorption in the night spectra (0200 and 2000 hours) because of the sharp near-surface inversion layer that forms at night. The expected radiance from an upward-looking spectrum is sub-

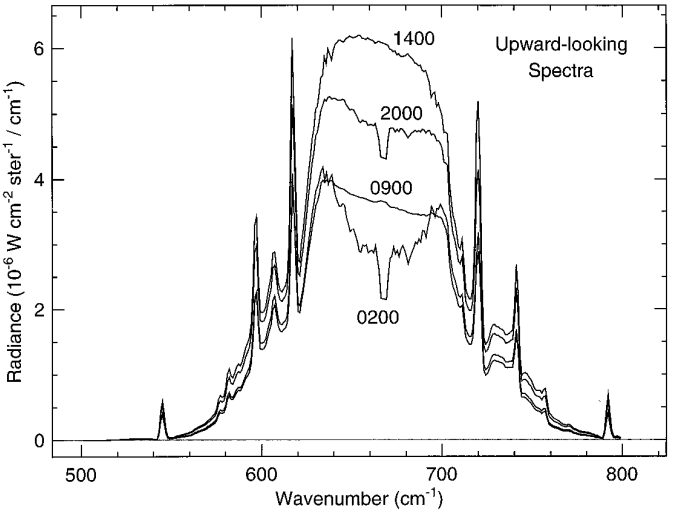

FIG. 3. Synthetic dust-free upward-looking Mars infrared spectra in the 667 cm^{-1} CO_2 band. Radiances are calculated using temperature profiles typical of various times during the Mars day, a path straight upward through the atmosphere toward zenith, and a spectral resolution of 2.8 cm^{-1}. A strong signal is apparent, showing large variation from day to night.

stantial, and exhibits large changes from day to night. Both the signal and its diurnal variation would easily be detected with high signal-to-noise by an instrument such as the Mariner 9 IRIS spectrometer.

c. Weighting Functions

A very useful quantity in describing radiative transfer through an atmosphere is the weighting function, W

$$W(\nu, s) = \frac{\partial}{\partial s}\left[\int \phi(\nu, \nu')e^{-\tau(\nu', s)}\, d\nu'\right], \tag{1}$$

where $\tau(\nu', s)$ is the optical depth, s is the coordinate that describes distance along the path, and $\phi(\nu, \nu')$ is the instrument spectral response function at frequency ν' when the central frequency is ν. The weighting function describes where the observed radiation originates along the viewing path, and it is a function both of the frequency, ν, and the distance coordinate, s. For a non-scattering atmosphere in local thermodynamic equilibrium, the total radiation observed by an instrument over a small solid angle is just

$$I(\nu) = \int_0^\infty B[\nu, T(s)]W(\nu, s)\, ds, \tag{2}$$

where B is the Planck function. The locations where W is largest are the locations from where the contribution to the observed radiation is largest. To retrieve a temperature profile from observations, it is desirable to choose a set of frequencies such that their weighting functions are peaked at different heights in the atmosphere and have minimal overlap with each other. Then, the radiance at a given frequency (and thus a temperature) can be assigned to a certain level in the atmosphere with a minimal amount of contamination from other levels.

Considering an upward-looking geometry with a path vertically upward through the atmosphere toward zenith, the variable s could be just the linear height above the surface, z, but it could also be any function of z by performing a change of variables for the vertical coordinate. A common choice for s is to measure distance in scale heights, $s = \hat{z} \equiv \ln(p_{\text{surf}}/p)$. Figure 4a shows weighting functions with the choice $s = \hat{z}$ for a set of frequencies in the 667-cm^{-1} CO_2 band for a nominal afternoon temperature profile. All weighting functions are sharply peaked at the surface. This is far from the ideal case for temperature retrieval described above. In this coordinate system, the weighting functions are very similar, and the retrieval of a temperature profile depends on the small differences between the shapes of the weighting functions. This is numerically difficult and leads to instability in the retrieval and/or large errors in the retrieved temperature profiles.

We desire a coordinate that provides weighting functions

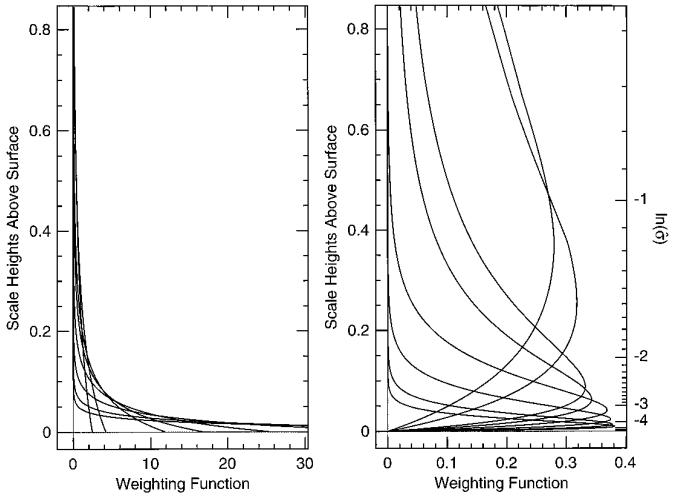

FIG. 4. Weighting functions for a typical daytime Mars temperature profile. In both plots, the central frequencies are 670, 675, 684, 690, 696, 700, 704, and 709 cm^{-1} from the bottom up. The left panel (a) shows weighting functions with respect to the distance coordinate $\hat{z} = \ln(p_{\text{surf}}/p)$. These weighting functions are not well suited for temperature retrieval. The right panel (b) shows weighting functions with respect to the distance coordinate $s = \ln \hat{\sigma} \equiv \ln[(p_{\text{surf}} - p)/p_{\text{surf}}]$. These weighting functions have peaks at different values of the vertical coordinate and are therefore much better suited for temperature retrieval.

that are as suitable for temperature retrieval as those used in analysis of downward-looking spectra. In that case, a log-pressure (or distance in scale heights) vertical coordinate is usually used, so that the coordinate is proportional to the logarithm of the pressure difference between the observer and a point along the path. For the upward-looking case, the observer is no longer at zero pressure, but at the surface pressure, p_{surf}. Thus, an analogous coordinate for this case is $s' = \ln \hat{\sigma} \equiv \ln[(p_{\text{surf}} - p)/p_{\text{surf}}]$. The column-integrated mass of the gas through which a path passes (in the zenith geometry) is proportional to the pressure difference between the ends of the path, so both coordinates (log-pressure for downward-looking and $\ln \hat{\sigma}$ for upward-looking) are proportional to the log of the mass of the gas between the observer and a point along the path, and both provide weighting functions that are well suited for temperature retrieval.

The coordinate, $s' = \ln \hat{\sigma}$, can be related to the previously discussed coordinate, $s = \hat{z}$, as follows. From Eq. (1), we have

$$W(\nu, s)\, ds = W'(\nu, s')\, ds'. \tag{3}$$

This means that the new weighting functions, $W'(\nu, \ln \hat{\sigma})$, are related to the old weighting functions, $W(\nu, \hat{z})$, by

$$W'(\nu, \ln \hat{\sigma}) = \frac{d\hat{z}}{d \ln \hat{\sigma}} W(\nu, \hat{z}) \tag{4}$$

or,

$$W'(\nu, \ln \hat{\sigma}) = \frac{p_{\text{surf}} - p}{p} W(\nu, \hat{z}). \quad (5)$$

Figure 4b shows the transformed weighting functions, $W'(\nu, \ln \hat{\sigma})$, with respect to the coordinate $\ln \hat{\sigma}$. These weighting functions are much more suitable for temperature retrieval. Although there is still a fair amount of overlap between them, the overlap is considerably less than that in Fig. 4a, and most importantly, each weighting function has a relatively narrow peak at a different value of the coordinate. By transforming to the $\ln \hat{\sigma}$ coordinate system we have "stretched out" the coordinate close to the surface and have thus mathematically separated the level of maximum influence for the different frequencies. We use this $\ln \hat{\sigma}$ vertical coordinate in our retrieval algorithm.

3. RETRIEVAL ALGORITHM

a. Retrieval General Description

For our retrieval we use the 667-cm^{-1} CO_2 absorption band. This band is extremely strong, lies near the peak of the martian thermal emission, and is virtually free from contamination by H_2O or other gaseous species (Crisp 1990). There is significant opacity (see Fig. 3) between about 600 and 730 cm^{-1}. Thermal infrared spectrometers flown on spacecraft typically have spectral resolution of about 3–10 cm^{-1}, as do, for example, the Mariner 9 IRIS instrument (Hanel *et al.* 1972) and the Thermal Emission Spectrometer to be flown on the Mars Global Surveyor mission (Christensen *et al.* 1992). Therefore, sampling of up to about 20 different frequencies on each side of the CO_2 band would be possible. In this paper we use just 8 different frequencies (670, 675, 684, 690, 696, 700, 704, and 709 cm^{-1}) with a spectral spacing of at least 4 cm^{-1} between each frequency.

To perform the retrieval, we follow the approach of Conrath *et al.* (1994) who used a constrained and linearized least-squares inversion of the equations of radiative transfer to simultaneously retrieve temperature and the *para* hydrogen fraction from Voyager infrared spectra of the outer planets. The problem of retrieving a temperature profile from a spectrum is in general ill-posed, so some *a priori* assumptions need to be made to obtain a physically meaningful solution. In this formulation the assumption takes the form of a constraint that acts as a low-pass filter (in the vertical coordinate) on the temperature profile. The tradeoff here is between increased vertical resolution and decreased temperature error (Conrath 1972). The balance is struck by varying parameters until a maximum vertical resolution is obtained while retaining an acceptable temperature error.

b. Retrieval Equations and Algorithm

We begin by taking Eq. (2), the expression for the observed radiance, $I(\nu)$, given a non-scattering atmosphere in local thermodynamic equilibrium, and linearizing about a reference temperature profile, $T_0(s)$,

$$I(\nu) = I_0(\nu) + \Delta I(\nu) \quad (6)$$

$$I_0(\nu) = \int_0^\infty B[\nu, T_0(s)] W(\nu, s)\, ds. \quad (7)$$

In finite difference form, if we have frequencies, ν_i with $(i = 1, \ldots, m)$, and vertical levels, s_j with $(j = 1, \ldots, n)$, then

$$\Delta I(\nu_i) = \sum_{j=1}^{n} \frac{\delta I_i}{\delta T_j} \Delta T_j, \quad (8)$$

where $\delta I_i / \delta T_j$ is the value of the functional derivative of the radiance at ν_i with respect to T at level s_j, with $s_j = \ln \hat{\sigma}_j \equiv \ln[(p_{\text{surf}} - p_j)/p_{\text{surf}}]$ and $\Delta T_j = T(s_j) - T_0(s_j)$.

The vector of ΔT_j values can in general be expressed in terms of a set of basis vectors,

$$\mathbf{\Delta T} = \mathbf{Fa}, \quad (9)$$

where $\mathbf{F}$ is a matrix whose columns are the basis vectors, $\mathbf{a}$ is a column vector of expansion coefficients, and $\mathbf{\Delta T}$ is a column vector of ΔT_j values. If we define the matrix $\mathbf{K}$ as,

$$K_{ij} = \frac{\delta I_i}{\delta T_j} \quad (10)$$

and if we use Eq. (9) for $\mathbf{\Delta T}$, then we can write an expression for a quadratic form, Q, to be minimized in our constrained and linearized least-squares inversion of Eq. (8):

$$Q = (\mathbf{\Delta I} - \mathbf{KFa})^{\mathrm{T}} \mathbf{E}^{-1} (\mathbf{\Delta I} - \mathbf{KFa}) + \gamma \mathbf{a}^{\mathrm{T}} \mathbf{a}. \quad (11)$$

Here, $\mathbf{E}$ is the error covariance matrix, $\mathbf{\Delta I}$ is the difference between the observed radiance and the radiance calculated by using the reference temperature profile, and the superscript "T" denotes matrix transposition. The last term in Eq. (11) imposes a damping, scaled through the parameter, γ, which limits the amount that the temperature can be different from the reference profile, T_0. If we make the assumption that errors are statistically independent, then

$$\mathbf{E} = \sigma_I^2 \mathbf{1}, \quad (12)$$

where σ_I is the noise-equivalent radiance (taken here as independent of frequency), and **1** is the unit matrix. Minimizing Q with respect to T_j, and solving for **a** gives,

$$\mathbf{a} = \frac{1}{\gamma\sigma_I^2}\mathbf{F}^{\mathrm{T}}\mathbf{K}^{\mathrm{T}}\left(\frac{1}{\gamma\sigma_I^2}\mathbf{K}\mathbf{F}\mathbf{F}^{\mathrm{T}}\mathbf{K}^{\mathrm{T}} + \mathbf{1}\right)^{-1}\mathbf{\Delta I}. \tag{13}$$

Finally, defining the 2-point correlation matrix, **S**, of the basis vectors,

$$\mathbf{S} = \mathbf{F}\mathbf{F}^{\mathrm{T}} \tag{14}$$

and a parameter, α,

$$\alpha = \frac{1}{\gamma\sigma_I^2} \tag{15}$$

and solving for the vector $\mathbf{\Delta T}$ using Eqs. (9) and (13) gives,

$$\mathbf{\Delta T} = \alpha\mathbf{S}\mathbf{K}^{\mathrm{T}}(\alpha\mathbf{K}\mathbf{S}\mathbf{K}^{\mathrm{T}} + 1)^{-1}\mathbf{\Delta I}. \tag{16}$$

Equation 16 prescribes the correction to the temperature profile T_j given (1) the difference, $\mathbf{\Delta I}$, between the observed radiance and the radiance calculated by using the reference temperature profile, and (2) the constraints imposed by the parameter α. Non-linearity in Eq. (5) can be accounted for by iteratively correcting the reference temperature profile by the amount $\mathbf{\Delta T}$.

c. Parameters

The parameters that need to be specified for this retrieval are (1) the 2-point correlation matrix of the basis vectors, **S**, (2) an initial guess of the temperature profile (the "reference temperature profile," T_0, discussed above), and (3) the combination of the damping parameter and radiance measurement uncertainty, α. We assume that there is no dust in the atmosphere, and that the spectra are taken with a viewing geometry looking directly upward through the atmosphere toward zenith.

The vertical resolution of the retrieval is set through the 2-point correlation matrix of the basis vectors, **S**, defined in Eq. (14). This matrix describes the degree of correlation between two atmospheric levels. If **S** were the unit matrix, then there would be no correlation between different levels and Eq. (16) would become equivalent to linearized maximum entropy algorithms. For our retrieval scheme, however, we wish to impose a correlation between nearby levels to reduce temperature errors caused by random instrument noise. The shape of the weighting functions gives the fundamental vertical resolution of radiative transfer. The typical width of the weighting functions with respect to the coordinate s (Fig. 4b), is about $\Delta s = \Delta \ln \hat{\sigma} = 2$.

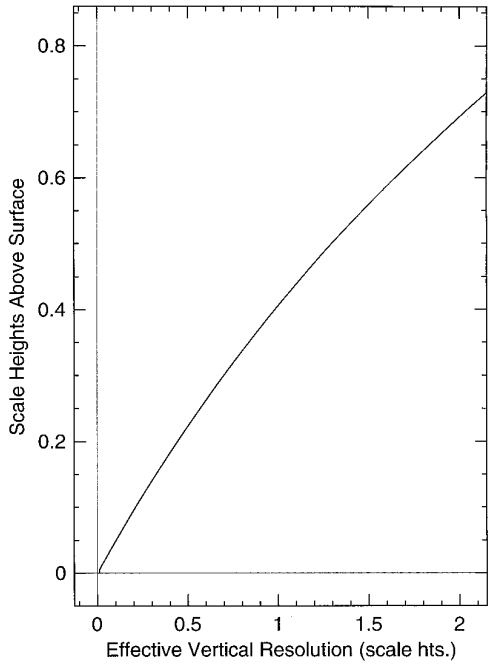

FIG. 5. Effective vertical resolution using the 2-point correlation function of Eq. (14b). The effective vertical resolution is a function of height with the resolution being approximately equal to twice the height above the surface.

Therefore, for two layers m and n, it is appropriate to express **S** as a Gaussian with the form

$$S_{mn} = e^{-(s_m - s_n)^2/2w^2}, \tag{17a}$$

where w is the weighting function width with respect to the coordinate s and is approximately equal to two. In practice, we modify Eq. (17a) slightly because the lowest weighting function peaks at 0.01 scale heights above the ground ($s = -4.6$), but the bottom of our model atmosphere is at $s = -8$. Since there is very little retrievable information below the peak of the lowest weighting function, the correlation matrix is set to the greater of Eq. (17a), or a Gaussian with width equal to 0.01 scale heights,

$$S_{mn} = \max(e^{-(s_m - s_n)^2/2w_s^2}, e^{-(\hat{z}_m - \hat{z}_n)^2/2w_{\hat{z}}^2}), \tag{17b}$$

where $\hat{z}$ is the height above the ground in local scale heights, as before, and the Gaussian widths that we adopt are $w_s = 2$ and $w_{\hat{z}} = 0.01$. Figure 5 shows the effective vertical resolution obtained using Eq. (17b). The effective vertical resolution is approximately equal to twice the distance above the surface, except that it is 0.01 scale heights for altitudes less than 0.01 scale heights.

The temperature profile that we use to initialize all our retrievals is taken to be

$$T_0(\hat{z}) = 235 - 35\hat{z}. \quad (18)$$

This profile is similar to those shown in Fig. 1, but it is not the same as any of them. Numerical experiments show that the retrieved temperature where there is significant amplitude in the weighting functions (between about 0.01 and 0.8 scale heights above the surface) is not sensitive to the choice for T_0. Convergence is obtained more quickly for better choices of T_0, so a good guess for the initial temperature profile is always desirable.

The parameter α contains the damping parameter, γ, that controls how large $\mathbf{\Delta T}$ can be, in addition to the uncertainty of the radiance measurement, σ_I. Based on experience with the Mariner 9 IRIS and Mars Observer Thermal Emission Spectrometer instruments, we take $\sigma_I = 3 \times 10^{-8}$ W cm^{-2} ster^{-1}/cm^{-1} as a conservative (noisy) estimate. The optimum value for γ is found by conducting numerical experiments. The balance here is between faster convergence and numerical stability. Small values of γ allow the temperature profile to quickly converge, but can also lead to numerical instability. Large values of γ provide a stable retrieval but may require considerable computational resources. We find that the choice $\gamma \approx 10$ (degrees K)$^{-2}$ is a good compromise. This makes the parameter $\alpha = 10^{16}$ if radiance is measured in W cm^{-2} ster^{-1}/cm^{-1} and temperature is in degrees K.

d. *Synthetic Spectra* (*Simulated Data*)

The upward-looking infrared spectral ''observations'' from which temperature profiles are retrieved in this paper are computed by numerically integrating Eq. (2). The temperature profiles are those given in Section 2a (see Fig. 1). For the nominal case we assume a non-scattering, dust-free atmosphere. Opacity in the 667 cm^{-1} CO_2 band is treated using the correlated-k approximation (Lacis and Oinas 1991, Goody *et al.* 1989). Instead of performing a line-by-line calculation, the idea behind the correlated-k approximation is to sort the absorption coefficient values, k (where $d\tau = -kdz$), in a spectral interval $[\nu, \nu + \Delta\nu]$ into n bins, and then to perform the radiative transfer integral (Eq. (2)) using a single value of k_i characteristic of each bin ($i = 1, 2, 3, \ldots, n$). The results are then added together weighted by the fraction of the spectral interval for which the absorption coefficient k is in each bin. The chosen k_i values are a function of temperature, pressure, and spectral resolution $\Delta\nu$.

e. *Solution*

To numerically evaluate the temperature correction given by Eq. (16), we construct a plane-parallel model atmosphere consisting of 200 layers. We use layers that are evenly spaced in the coordinate $s = \ln \hat{\sigma}$ in the range from $s = -8$ (3.35×10^{-4} scale heights above the ground) to $s = 0$ (infinitely high), making the model layer thickness approximately 1/50th of the best effective vertical resolution which is attained near the surface. We assume that temperature is constant in each layer and that there are no horizontal variations. The correlation and functional derivative matrices are computed in finite difference form, and the temperature correction is computed for each model layer. Typically, three iterations are sufficient for convergence with our choice of parameters.

4. RESULTS

a. *Retrieved Temperatures Using Nominal Parameters*

Figure 6 shows retrieved temperature profiles for nine times during the martian day. The growth and collapse of the near-surface boundary layer is duplicated in depth and amplitude in the retrievals. There is significant difference in the shape of weighting functions between about 0.01 and 0.5 scale heights above the surface, and so this is the region where the retrieved profiles are reliable. Fine detail, such as the small local temperature minimum that occurs at 0900 hours in the ''actual'' profile is not present in the retrieved profile because its vertical scale is too small for this retrieval to detect. Many of the retrieved profiles show a sharp temperature increase in the lowest 0.01 scale height above the surface. This is an artifact of the retrieval introduced by the initial guess temperature profile. Its presence has negligible effect on studies of the PBL utilizing our inversions.

b. *Variation with the Correlation Length Scale*

Figure 7 shows how the retrieved temperature profiles change when the 2-point correlation length scale, w_s, is varied. Results are shown for two representative times of day. At night (0200 hours), variation in w_s strongly affects the retrievals. The $w_s = 4$ profile does not retain enough vertical resolution to accurately describe the inversion in the lowest kilometer. The $w_s = 0.5$ and $w_s = 1$ profiles have sufficient vertical resolution to duplicate the actual temperature profile, but the random temperature error associated with those values of w_s is relatively large. The nominal choice of $w_s = 2$ provides the most accurate retrieval. It is the best compromise between high vertical resolution and small random temperature errors. During the afternoon (1400 hours), the actual temperature profile does not contain any features with small vertical length scale except for the mild ''kink'' in the profile just above 0.4 scale heights. In this case, all four choices for w_s do similarly well. The $w_s = 4$ profile is good because the retrieval does not need high vertical resolution, and the

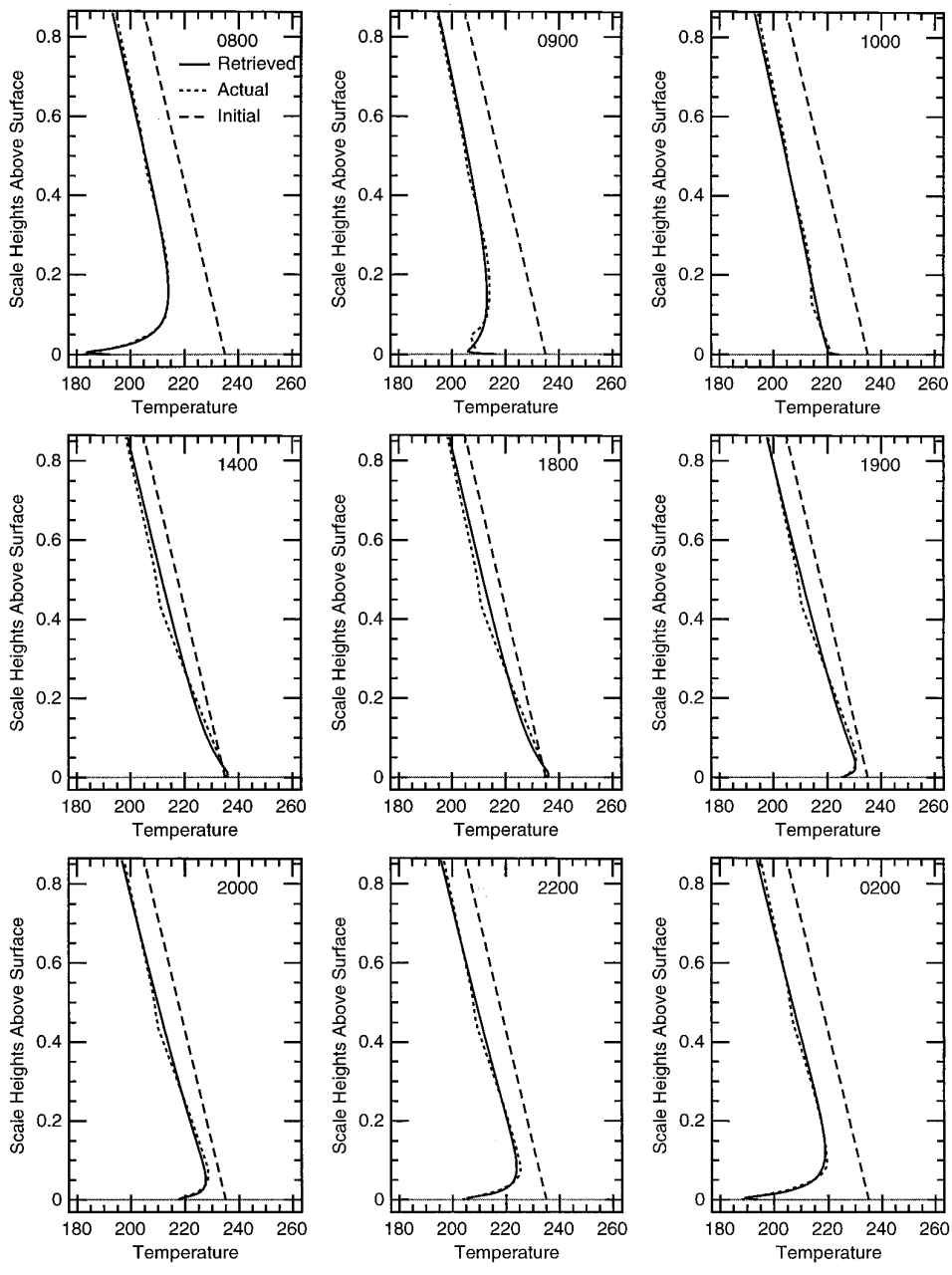

FIG. 6. Retrieved temperature profiles for nine times during the martian day using nominal parameters.

large random errors evident in the nighttime $w_s = 0.5$ retrieval do not appear in the daytime $w_s = 0.5$ profile because the actual temperature profile is similar to the initial guess temperature profile.

c. Variation with the Parameter α

Figure 8 shows how the retrieved temperature profiles change when α is varied. The parameter α (Eq. (15)) contains the damping parameter γ that controls by how much the temperature profile is allowed to change ($\mathbf{\Delta T}$) in any one iteration, as well as the uncertainty in the radiance measurement. In each case shown, three iterations have been performed, and the instrument uncertainty is held fixed so that variation of α is caused only by a change in γ. The $\alpha = 10^{12}$ case represents a very strong constraint on $\mathbf{\Delta T}$. After three iterations the retrieved temperature profile is essentially the same as the initial guess. At $\alpha = 10^{14}$, the constraint on $\mathbf{\Delta T}$ has been relaxed, but still keeps the retrieved temperature profile from reaching convergence in three iterations. In both of these cases, the re-

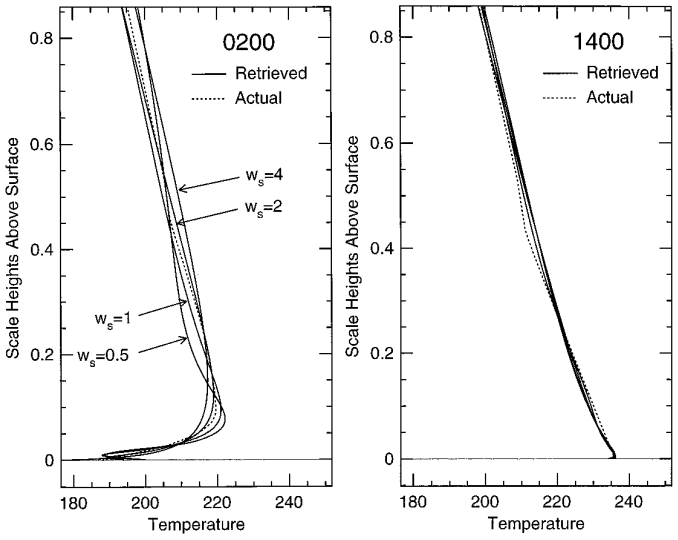

FIG. 7. Retrieved temperature profiles for four values of the 2-point correlation length scale, w_s. The nominal value is $w_s = 2$. Results for typical night (0200 hours) and day (1400 hours) cases are shown.

trieval would reach convergence eventually, but would require more than three iterations. Using the nominal value of $\alpha = 10^{16}$ results in convergence in three iterations. However, increasing α significantly beyond the nominal value (such as to $\alpha = 10^{18}$) results in the retrieval becoming numerically unstable. The beginning of instability is apparent in Fig. 8 for $\alpha = 10^{18}$, and more iterations lead to retrieved profiles further from the actual profile.

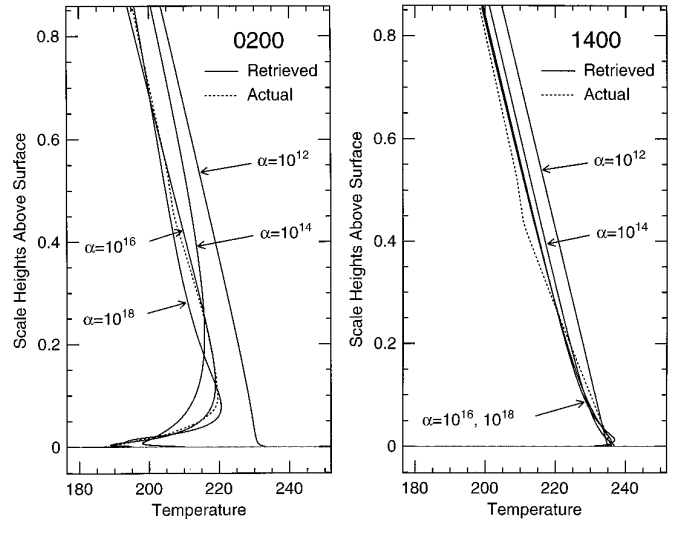

FIG. 8. Retrieved temperature profiles for four values of the parameter, α. The nominal value is $\alpha = 10^{16}$. Results for typical night (0200 hours) and day (1400 hours) cases are shown.

5. DISCUSSION

a. Propagation of Uncertainty

We have made approximations and assumptions about the atmosphere and computational parameters to perform the above retrievals. However, the only source of random error in the expression for the temperature correction (Eq. (16)) comes from the uncertainty in the radiance measurement by the spectrometer, σ_I. We can estimate the effect of this measurement error on retrieved temperatures. This gives a measure of the reproducibility of temperature retrievals given different spectra observed by the same instrument under the same conditions. We first define the matrix $\mathbf{C}$,

$$\mathbf{C} = \alpha\mathbf{S}\mathbf{K}^{\mathrm{T}}(\alpha\mathbf{K}\mathbf{S}\mathbf{K}^{\mathrm{T}} + \mathbf{1})^{-1} \tag{19}$$

so that we can write for a given atmospheric layer, j,

$$\Delta T_j = \sum_i C_{ij}\,\Delta I_i, \tag{20}$$

where the sum is performed over frequencies, i. If the uncertainty in the radiance measurement is a constant σ_I for all frequencies, i, then the root-mean-square (RMS) temperature error at level j is

$$[\langle \delta T_j^2 \rangle]^{1/2} = \left[\sum_i C_{ij}^2\right]^{1/2} \sigma_I. \tag{21}$$

Using $\sigma_I = 3 \times 10^{-8}$ W cm^{-2} ster^{-1}/cm^{-1}, a conservative estimate for a future instrument, we find that the temperature uncertainty caused by instrument noise is less than 0.7 K at all levels. Other errors of a systematic nature are also present in the retrieval, such as those caused by calibration or by using the 2-point correlation function. Recalling Fig. 6 indicates that these systematic errors dominate the random error from instrument noise.

b. Atmospheric Dust and Water Ice Aerosols

Dust particles are always present in the martian atmosphere. In the above analysis, however, we have assumed that the effect of dust is negligible at the frequencies that we have been considering. Usually this assumption is a good one, but during the global dust storms that occur irregularly every few years, dust can contribute significantly to infrared opacity even in the 667 cm^{-1} CO_2 band, and it can greatly alter atmospheric temperatures by increasing direct solar heating. We attempt to estimate the error caused by not including dust by adding a well-mixed non-scattering absorber to our model. We take the frequency dependence of this "dust" opacity to be that of palagonite (Roush *et al.* 1991). The exact mineral used is

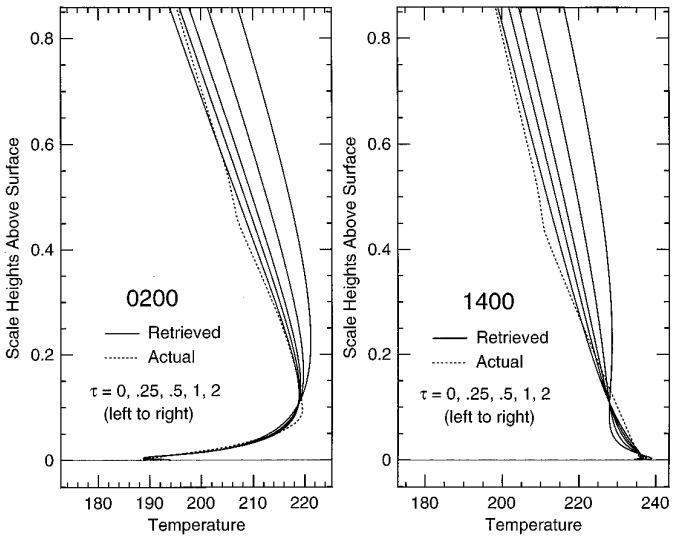

FIG. 9. Retrieved temperature profiles for five optical depths of dust, τ. Results for typical night (0200 hours) and day (1400 hours) cases are shown.

not important here since only an estimate of the importance of dust is being attempted. We perform the retrieval as before, still assuming that CO_2 is the only source of opacity, even though a dust component has been added in evaluating the ''observed'' radiances. Figure 9 shows the results of the retrievals for five different amounts of dust. The optical depth of the dust, τ, refers to the average optical depth between 1000 and 1100 cm^{-1} where dust opacity is the greatest. The optical depth near 700 cm^{-1}, where the retrieval takes place, is about 40% of that value. A value of $\tau = 0.25$ is typical of normal, ''non-dusty'' times (Martin 1986; Santee and Crisp 1993), while during a global dust storm $\tau \geq 2$ (Zurek 1982). The addition of dust tends to increase the retrieved temperature at each level, by about 1 degree for $\tau = 0.25$ and by about 10 degrees for $\tau = 2$. This is because the added opacity places the level where total optical depth (CO_2 plus dust) equals unity lower in the atmosphere since we are looking upward from the surface. This means that the observation sees a higher radiance than expected for pure CO_2 (at least where temperature decreases with height), and thus a higher temperature is assigned by the retrieval. The effect of adding dust is small in the lowest kilometer or so, but grows rapidly with height. This is because near the surface the retrieval is sensitive to frequencies with very high total column optical depth, so the additional opacity from dust is small compared to the opacity from CO_2. At higher altitudes the retrieval is sensitive to frequencies with lower total column optical depth and the additional opacity from dust can be a significant fraction of the opacity from CO_2. For non-dusty conditions ($\tau \leq 0.25$), the errors introduced by neglecting dust are not too much more than the RMS error caused by instrument noise or that caused by other systematic errors. However, for times when the dust opacity is higher, a simultaneous retrieval of temperature and dust optical depth (as was performed by Santee and Crisp 1993, for example) would be required to produce accurate temperature profiles. Scattering by dust would introduce further error by scattering photons from the surface back to the instrument. However, the single scattering albedo of palagonite is quite low (0.1–0.2) at the frequencies used for this retrieval and for typical dust particle size distributions (Toon *et al.* 1977, Santee and Crisp 1993), so the temperature error due to scattering by dust is small compared to that due to dust absorption and re-emission described above.

Besides dust aerosols, the other potentially significant source of opacity is from water ice aerosols. Pollack *et al.* (1977) observed a ground fog made of water ice particles in nighttime Viking Lander data. A nighttime fog near the ground is also present in planetary boundary layer models (Savijärvi 1995). The signature of higher level ice clouds is observed in a number of Mariner 9 infrared spectra (Curran *et al.* 1973), and ice clouds are seen in images taken by Mariner 9 (Briggs and Leovy 1974) and Viking (Kahn 1984). In the Mariner 9 spectra (Curran *et al.* 1973), the spectral signature of H_2O ice is quite different than that of CO_2 and dust, so as is the case with dust, H_2O ice can be identified, and its opacity simultaneously retrieved with temperature if it is present.

c. Using a Different Path Geometry

An important feature for a lander-based spectrometer would be the ability to take spectra at a range of viewing angles, from directly upward toward zenith to sideways toward the horizon. We can describe the viewing angle in terms of the airmass, a, defined as the opacity along the line of sight divided by the opacity along a path directly upward toward zenith. For a plane-parallel atmosphere the airmass is simply

$$a = \frac{1}{\cos\theta}, \tag{22}$$

where θ is the angle between the line of sight and zenith. In a real spherical atmosphere, a maximum airmass of about 20 is reached looking directly toward the horizon ($\theta = 90°$). Although the height above the surface of the peak of a particular weighting function varies roughly as $\sqrt{a}$ for downward-looking geometry, the peak height varies roughly as $1/a$ for the upward-looking geometry. It follows then that the range of useful information is shifted downward, and that the vertical length scale in kilometers (or scale heights) that can effectively be resolved is de-

creased, by a factor of a. Actually computing the weighting functions as a function of a shows this approximation to be good.

The advantage of using a viewing angle more toward the horizon is that a longer path length of atmosphere is viewed. Using viewing angles with high airmass would aid in the detection and study of trace atmospheric constituents, as well as in the study of near-surface phenomena. Observations over a range of viewing angles would likely give better constraints on the scattering properties of atmospheric aerosols, and could provide information on the vertical distribution of fogs and hazes. The development of retrieval algorithms to take advantage of the additional information available from a set of spectra with a range of viewing angles would be a very useful addition to this retrieval.

d. General Comments

Although no upward-looking spectra taken from the surface of Mars currently exist, there are terrestrial upward-looking spectra of oxygen in the microwave region (52–59 GHz) that have been used to obtain temperature profiles in the lowest few kilometers of the Earth's atmosphere (Westwater 1972). The vertical coordinate used for these retrievals is the linear distance above the ground ($s = z$). This gives weighting functions that are very similar to those in Fig. 4a for $s = \hat{z}$. Instead of our damping constraint, γ, and use of the 2-point correlation matrix, these retrievals use constraints based on a large database of previous observations from weather balloons, a type of supporting data which would not be available for Mars. More recently, ground-based upward-looking microwave data have been combined with downward-looking spectra taken from orbit to obtain accurate temperature profiles over a wide range of altitudes (for example, Westwater *et al.* 1985, and the review by Askne and Westwater 1986). A similar scheme is desirable for Mars. A lander can retrieve temperatures in the lowest few kilometers, while an orbiter simultaneously retrieves temperatures above the PBL. The retrieved temperatures from each instrument (lander and orbiter) can then be used to constrain the retrievals of the other.

A lander taking upward-looking spectra has one key disadvantage to an orbiter taking downward-looking spectra. While an orbiter such as the Mars Global Surveyor can easily retrieve temperature profiles for a wide range of latitude and longitude, a conventional lander is fixed at one particular location. To alleviate this limitation, it would be desirable to have a network of landers.

6. SUMMARY

The coordinated use of both upward-looking and downward-looking thermal infrared spectra for temperature retrieval is desirable to obtain the most information possible about temperatures throughout the atmosphere. While retrievals using downward-looking spectra give a good overall view of the vertical temperature structure, they fail to provide significant information on the rapidly changing (in time and space) temperatures of the planetary boundary layer. We have provided a retrieval method using upward-looking spectra to fill this need.

As with retrievals using downward-looking spectra, the variation of opacity with frequency in the 667-cm^{-1} CO_2 band is employed for the upward-looking retrieval. A change of variables in the vertical coordinate allows the retrieval to be mathematically efficient. Tests with synthetic data from expected temperature profiles show that the major features of the diurnal cycle of the PBL can be obtained using upward-looking spectra. The useful vertical range for retrieved temperatures is between about 0.01 and 0.5 scale heights (100 m to 5.5 km) above the surface for nominal parameters. The effective vertical resolution varies with height, being roughly equivalent to twice the distance above the ground. Using a viewing angle more toward the horizon compresses the useful vertical range for retrieved temperatures and allows better vertical resolution. The propagation of instrument noise leads to a relatively small temperature uncertainty, and the major source of retrieved temperature error is systematic error in the retrieval process. Opacity from sources other than from CO_2, such as from dust and water ice aerosols, can be large, but these are potentially correctable by simultaneously retrieving temperature and aerosol abundance.

Logical extensions of this work would be to add a simultaneous retrieval for atmospheric aerosols, and to develop algorithms to take advantage of a set of spectra with a range of viewing angles. The extensive set of temperature profiles in the PBL that could be retrieved from a lander on the surface of Mars equipped with an infrared spectrometer would be a tremendous addition to the current limited set of PBL observations. The importance of these data, along with the possible addition of the retrieval of the abundance of dust and water ice aerosols, should be considered in the planning of future missions to Mars.

ACKNOWLEDGMENTS

M.D.S. is supported by the National Research Council postdoctoral associateship program. We thank Drs. T. Clancy and J. Murphy for improving this paper through their helpful reviews.

REFERENCES

Askne, J. I. H., and E. R. Westwater 1986. A review of ground-based remote sensing of temperature and moisture by passive microwave radiometers. *IEEE Trans. Geosci. Rem. Sens.* **GE–24,** 340–352.

Briggs, G. A, and C. B. Leovy 1974. Mariner 9 observations of the Mars north polar hood. *Bull. Amer. Meteorol. Soc.* **55,** 278–296.

Christensen, P. R., D. L. Anderson, S. C. Chase, R. N. Clark, H. H. Kieffer, M. C. Malin, J. C. Pearl, J. Carpenter, N. Bandiera, F. G. Brown, and S. Silverman 1992. Thermal emission spectrometer experiment: Mars observer mission. *J. Geophys. Res.* **97,** 7719–7734.

Conrath, B. J. 1972. Vertical resolution of temperature profiles obtained from remote radiation measurements. *J. Atmos. Sci.* **29,** 1262–1271.

Conrath, B. J. 1975. Thermal structure of the martian atmosphere during the dissipation of the dust storm of 1971. *Icarus* **24,** 36–46.

Conrath, B. J. 1981. Planetary-scale wave structure in the martian atmosphere. *Icarus* **48,** 246–255.

Conrath, B. J., P. J. Gierasch, M. D. Smith, and E. A. Ustinov 1994. Simultaneous retrieval of temperature and *para* hydrogen in Neptune's atmosphere. *Bull. Amer. Astron. Soc.* **26,** 1095.

Conrath, B. J., R. Curran, R. Hanel, V. Kunde, W. Maguire, J. Pearl, J. Pirraglia, and J. Welker 1973. Atmospheric and surface properties of Mars obtained by infrared spectroscopy on Mariner 9. *J. Geophys. Res.* **78,** 4267–4278.

Crisp, D. 1990. Infrared radiative transfer in the dust-free martian atmosphere. *J. Geophys. Res.* **95,** 14577–14588.

Curran, R. J., B. J. Conrath, R. A. Hanel, V. G. Kunde, and J. C. Pearl 1973. Mars: Mariner 9 spectroscopic evidence for H_2O ice clouds. *Science* **182,** 381–383.

Gierasch, P. J., and R. Goody 1967. An approximate calculation of radiative heating and radiative equilibrium in the martian atmosphere. *Planet. Space Sci.* **15,** 1465–1477.

Gierasch, P. J., and R. Goody 1968. A study of the thermal and dynamical structure of the martian lower atmosphere. *Planet. Space Sci.* **16,** 615–646.

Goody, R., R. West, L. Chen, and D. Crisp 1989. The correlated-*k* method for radiation calculations in nonhomogeneous atmospheres. *J. Quant. Spectrosc. Radiat. Transfer* **42,** 539–550.

Haberle, R. M., H. C. Houben, R. Hertenstein, and T. Herdtle 1993. A boundary-layer model for Mars: Comparison with Viking Lander and entry data. *J. Atmos. Sci.* **50,** 1544–1559.

Hanel, R., B. Schlachman, E. Breihan, R. Bywaters, F. Chapman, M. Rhodes, D. Rodgers, and D. Vanous 1972a. Mariner 9 Michelson interferometer. *Appl. Opt.* **11,** 2625–2634.

Hanel, R., B. Conrath, W. Hovis, V. Kunde, P. Lowman, W. Maguire, J. Pearl, J. Pirraglia, C. Prabhakara, and B. Schlachman 1972b. Investigation of the martian environment by infrared spectroscopy on Mariner 9. *Icarus* **17,** 423–442.

Hess, S. L., R. M. Henry, C. B. Leovy, J. A. Ryan, and J. E. Tillman 1977. Meteorological results from the surface of Mars: Viking 1 and 2. *J. Geophys. Res.* **82,** 4559–4574.

Kahn, R. 1984. The spatial and seasonal distribution of martian clouds and some meteorological implications. *J. Geophys. Res.* **89,** 6671–6688.

Kliore, A. J., G. Fjeldbo, B. L. Seidel, M. J. Sykes, and P. M. Woiceshyn 1973. S band radio occultation measurements of the atmosphere and topography of Mars with Mariner 9: Extended mission coverage of polar and intermediate latitudes. *J. Geophys. Res.* **78,** 4331–4351.

Lacis, A. A., and V. Oinas 1991. A description of the correlated *k* distribution method for modeling nongray gaseous absorption, thermal emission, and multiple scattering in vertically inhomogeneous atmospheres. *J. Geophys. Res.* **96,** 9027–9063.

Lindal, G. F., H. B. Hotz, D. N. Sweetnam, Z. Shippony, J. P. Brenkle, G. V. Hartsell, and R. T. Spear 1979. Viking radio occultation measurements of the atmosphere and topography of Mars: Data acquired during 1 martian year of tracking. *J. Geophys. Res.* **84,** 8443–8456.

Martin, T. 1986. Thermal infrared opacity of the Mars atmosphere. *Icarus* **66,** 2–21.

Pollack, J. B., D. Colburn, R. Kahn, J. Hunter, W. Van Camp, C. E. Carlston, and M. R. Wolf 1977. Properties of aerosols in the martian atmosphere, as inferred from Viking Lander imaging data. *J. Geophys. Res.* **82,** 4479–4496.

Pollack, J. B., D. S. Colburn, F. M. Flasar, R. Kahn, C. E. Carlston, and D. Pidek 1979. Properties and effects of dust particles suspended in the martian atmosphere. *J. Geophys. Res.* **84,** 2929–2945.

Roush, T., J. Pollack, and J. Orenberg 1991. Derivation of midinfrared (5–25 μm) optical constants of some silicates and palagonite. *Icarus* **94,** 191–208.

Santee, M., and D. Crisp 1993. Thermal structure and dust loading of the martian atmosphere during late southern summer: Mariner 9 revisited. *J. Geophys. Res.* **98,** 3261–3279.

Savijärvi, H. 1991. A model study of the PBL structure on Mars and the Earth. *Beitr. Phys. Atmos.* **64,** 219–229.

Savijärvi, H. 1995. Mars boundary layer modeling: Diurnal moisture cycle and soil properties at the Viking Lander 1 site. *Icarus* **117,** 120–127.

Seiff, A., and D. B. Kirk 1977. Structure of the atmosphere of Mars in summer at mid-latitudes. *J. Geophys. Res.* **82,** 4364–4378.

Seiff, A. 1982. Post-Viking models for the structure of the summer atmosphere of Mars. *Adv. Space Res.* **2,** 3–17.

Sutton, J. L., C. B. Leovy, and J. E. Tillman 1978. Diurnal variations of the martian surface layer meteorological parameters during the first 45 sols at two Viking Lander sites. *J. Atmos. Sci.* **35,** 2346–2355.

Toon, O. B., J. B. Pollack, and C. Sagan 1977. Physical properties of the particles composing the martian dust storm of 1971–1972. *Icarus* **30,** 663–696.

Westwater, E. R. 1972. Ground-based determination of low altitude temperature profiles by microwaves. *Mon. Weather Rev.* **100,** 15–28.

Westwater, E. R., W. Zhenhui, N. C. Grody, and L. M. McMillin 1985. Remote sensing of temperature profiles from a combination of observations from the satellite-based microwave sounding unit and the ground-based profiler. *J. Atmos. Oceanic Tech.* **2,** 97–109.

Zurek, R. W. 1982. Martian great dust storms: An update. *Icarus* **50,** 288–310.